Energy Harvester Design for Intelligent Tyre Systems

Otso Jousimaa

School of Electrical Engineering

Thesis submitted for examination for the degree of Master of Science in Technology.
Espoo XX.XX.XXXX

Thesis supervisor:

Prof. Arto Visala

Thesis advisors:

M.Sc. Yi Xiong

D.Sc. (Tech.) Ari Tuononen

Aalto-yliopisto
Sähkötekniikan
korkeakoulu

AALTO UNIVERSITY
SCHOOL OF ELECTRICAL ENGINEERING

ABSTRACT OF THE
MASTER'S THESIS

Author: Otso Jousimaa

Title: Energy Harvester Design for Intelligent Tyre Systems

Date: XX.XX.XXXX Language: English Number of pages: 6+39

Department of Automation and Systems Technology

Professorship: Smart products

Supervisor: Prof. Arto Visala

Advisors: M.Sc. Yi Xiong, D.Sc. (Tech.) Ari Tuononen

Your abstract in English. Try to keep the abstract short; approximately 100 words should be enough. The abstract explains your research topic, the methods you have used, and the results you obtained. Your abstract in English. Try to keep the abstract short; approximately 100 words should be enough. The abstract explains your research topic, the methods you have used, and the results you obtained.
Your abstract in English. Try to keep the abstract short; approximately 100 words should be enough. The abstract explains your research topic, the methods you have used, and the results you obtained. Your abstract in English. Try to keep the abstract short; approximately 100 words should be enough. The abstract explains your research topic, the methods you have used, and the results you obtained.

Keywords: For keywords choose concepts that are central to your thesis

AALTO-YLIOPISTO
SÄHKÖTEKNIIKAN KORKEAKOULU

DIPLOMITYÖN
TIIVISTELMÄ

Tekijä: Otso Jousimaa

Työn nimi: Energy Harvester Design for Intelligent Tire Systems

Päivämäärä: XX.XX.XXXX Kieli: Englanti Sivumäärä: 6+39

Automaatio- ja systeemitekniikan laitos

Professuuri: Älykkäät tuotteet

Työn valvoja: Prof. Arto Visala

Työn ohjaajat: DI Yi Xiong, TkT Ari Tuononen

Tiivistelmässä on lyhyt selvitys (noin 100 sanaa) kirjoituksen tärkeimmästä sisällöstä: mitä ja miten on tutkittu, sekä mitä tuloksia on saatu. Tiivistelmässä on lyhyt selvitys (noin 100 sanaa) kirjoituksen tärkeimmästä sisällöstä: mitä ja miten on tutkittu, sekä mitä tuloksia on saatu.
Tiivistelmässä on lyhyt selvitys (noin 100 sanaa) kirjoituksen tärkeimmästä sisällöstä: mitä ja miten on tutkittu, sekä mitä tuloksia on saatu. Tiivistelmässä on lyhyt selvitys (noin 100 sanaa) kirjoituksen tärkeimmästä sisällöstä: mitä ja miten on tutkittu, sekä mitä tuloksia on saatu. Tiivistelmässä on lyhyt selvitys (noin 100 sanaa) kirjoituksen tärkeimmästä sisällöstä: mitä ja miten on tutkittu, sekä mitä tuloksia on saatu.

Avainsanat: Vastus, Resistanssi,
Lämpötila

Preface

I want to thank Professor Pirjo Professori and my instructor Olli Ohjaaja for their good and poor guidance.

Otaniemi, 16.1.2015

Eddie E. A. Engineer

Contents

Symbols and abbreviations

Symbols

$\mathbf{A}$	area
$\mathbf{B}$	magnetic flux density
c	speed of light in vacuum $\approx 3 \times 10^8$ [m/s]
ε	electromotive force
$\mathbf{F}$	mechanical force
$\mathbf{I}$	electrical current
$\mathbf{l}$	length
Φ_B	magnetic flux through loop area
ρ	resistivity
$\mathbf{P}$	power
$\mathbf{p}$	pressure
$\mathbf{U}$	input to system
$\mathbf{V}$	voltage
$\mathbf{Y}$	output from system
$\mathbf{Z}$	complex impedance

Operators

$\frac{\mathrm{d}}{\mathrm{d}t}$	derivative with respect to variable t
$\frac{\partial}{\partial t}$	partial derivative with respect to variable t
$\sum_i$	sum over index i

Abbreviations

AC	Alternating Current
BLE	Bluetooth Low Energy
DC	Direct Current
EMF	Electromotive Force
IC	Integrated Circuit
MEMS	Microelectromechanical Systems
MPPT	Maximum Power Point Tracking
PV	Photovoltaic
RF	Radio Frequency
SMPS	Switch-Mode Power Supply
TPMS	Tire Pressure Monitoring Sensors

1 Introduction

As technology advances, it has become possible to build small, light-weight and yet powerful sensor platforms which can communicate wirelessly with their environment. New kind of applications are being created using the possibilities given by these sensor platforms. A common feature with all of these devices is that they need power to function, even if the power needed is minuscule.

Traditionally wireless devices have been powered by batteries, but as the number of sensors increases, the cost of changing or charging batteries becomes significant part of cost of any system. This is especially relevant for the devices which are in hard-to-reach areas, such as inner parts of heavy machinery, walls of bridges and high rise buildings, remote environmental sensors et cetera. On some applications the life of the battery can become a limiting factor for the lifetime of entire sensor, if cost of installing new sensor is similar to cost of replacing the battery.

A new approach to powering the device is to harvest the energy from it's surroundings using ambient energy as the power source. Examples of such energy sources are solar, wind, temperature differentials, and vibration. The technology to utilise some of these power sources, such as wind and solar is already widely deployed and even used in the large-scale power production. On a smaller scale the demand for reliable and efficient solutions has been growing strongly with the advent of wireless low-power devices and a lot of research has focused on creating suitable technologies and devices for low-power energy harvesting.

This work focuses on powering one of such devices, namely a sensor inside a car tyre. The car tyre provides some unique challenges and opportunities, as there is a lot of energy available, but on the other hand operating conditions can be extremely harsh with large temperature ranges and extreme vibration and shocks especially in rougher road conditions.

Car tyre sensing itself has been in focus of a lot development lately, as legislation in the United States demands new tyres being fitted with a pressure sensor to warn drivers about the low pressure and related higher fuel consumption, wear on tyre and even elevated risk of accidents. European Union has also laws which require Tire Pressure Monitoring Sensors (TPMS) on new passenger cars.

This paper is based on my Master's Thesis which is still a work in progress. The next section has overview of car tyres and the operational environment inside them. A quick review on possible energy harvesting technologies is made, piezoelectric and electromagnetic energy harvesting are selected for in depth comparison. Two different approaches are used determining the applicability of energy harvesting method: electromagnetic generator is researched based on theoretical analysis and simulation while piezoelectric harvesting is researched using experimental methods.

Conclusion presents findings based on the theoretical and experimental research phases of the work and discusses future work to be done to validate findings of theoretic designs.

2 Background

2.1 Structure of a tyre

Tyres are composed of several layers with different functions. Figure 1 by Gent et al. [17] shows the layered structure. From outer tread to inner lining, the layers are:

Tread provides traction for driving, braking and cornering. Pattern and materials on tread is a compromise between wear resistance, traction, handling and rolling resistance

Belts provide mechanical strength, impact resistance and keep tyre from expanding under centrifugal forces.

Body ply provides strength to contain the air pressure.

Innerliner is a compound specifically designed to improve air retention in tyre.

In addition there are layers designed to improve tyre reliability, such as the belt wedge which reduces shear between belts.

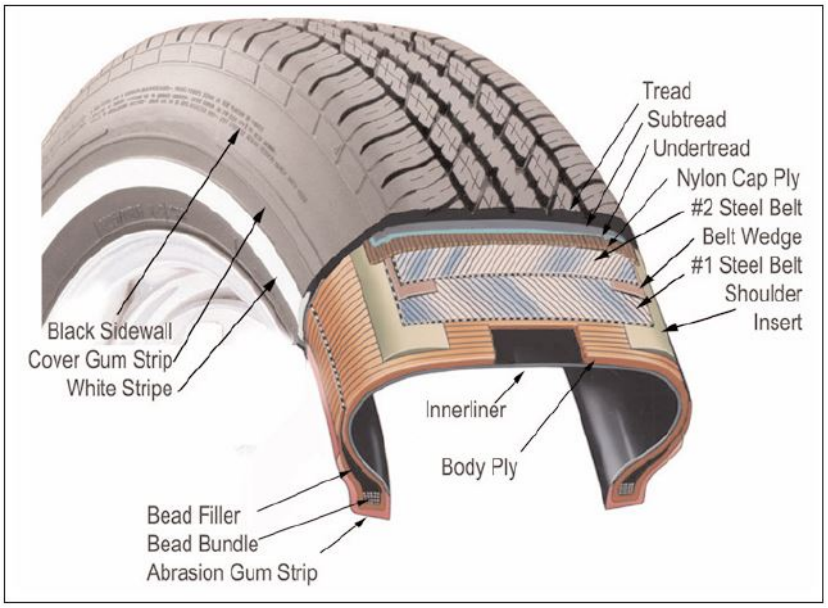

Figure 1: Structure of a tyre [17].

In endurance testing of tyres the car is driven at test track in three shifts until desired number of course driving kilometres have been reached. In outdoor testing each company has their own proprietary test protocol. Indoor testing has standards, which mandates pressure, ambient temperature and speed as well as time driven. According to Gent et al. [17] this indoor testing takes 34 hours of driving at 120 km/h.

In addition to endurance testing, there is high-speed testing where tyre speed is gradually accelerated in steps of 10 km/h at regular intervals until target speed is reached. Energy harvester should survive these tests to be considered a viable design for road conditions.

2.2 Environment inside tyre

The energy harvester will be placed inside the tyre. Previous studies by Niskanen et al [32]. have shown that the tyre will experience acceleration in all three axes. Tangential and centripetal accelerations are dominant, they can reach amplitudes up to 150 g in test fixture. In addition a study done by Löhndorf et al. [26] shows shock survival of up to 4 000 - 5 000 g is required for reliability.

Temperature inside of the tyre will reach equilibrium in ambient + 5-10 °C, so operation temperature should be in range of -40 to + 75 °C to have some safety margin on top of usual ambient conditions.

Previous work by Niskanen et al. [32] was used to as a basis for analysis of characteristics of acceleration inside the tyre. Raw data was used to gather minimum and maximum values of acceleration as well as frequency components inside tyre. Data was gathered at 20 km/h, 60 km/h and 80 km/h speeds. Figure 3 shows time domain representations of the acceleration along 3 axes as shown in figure 2.

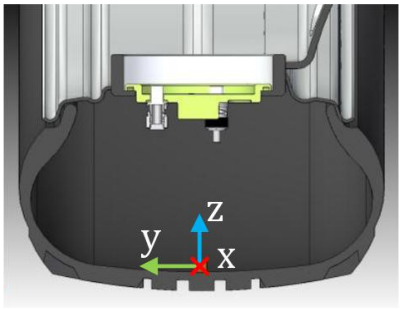

Figure 2: Axes in measurement by Matilainen et al. [28]

Frequency domain representations were calculated in Matlab. There are two main contributors to base frequencies: first is the rotational frequency of tyre itself and second is the impact when the tyre deforms as it contacts the drum.. There is clearly visible series of frequency components spaced at the rotational frequency of tyre as well as shock harmonics at upper frequencies. Figure 4 shows the total frequency spectrum and the dominant frequency components.

It's important to notice that the sensor used was piezoelectric, which forms a highpass filter as the operation of sensor is based on charge between layers. This charge dissipates over time, so the steady-state centripetal acceleration reads as zero. Any device on the rotating tyre will experience centripetal acceleration (acceleration toward centre of rotation) at the amplitude of:

$$a_{centripetal} = \omega^2 r, \tag{1}$$

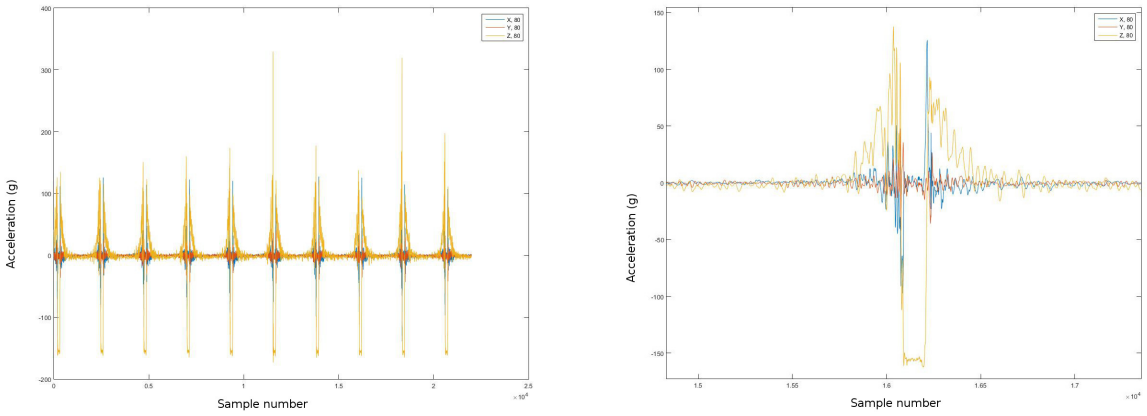

Figure 3: Acceleration of inner lining of tyre at 80 km/h in time domain.

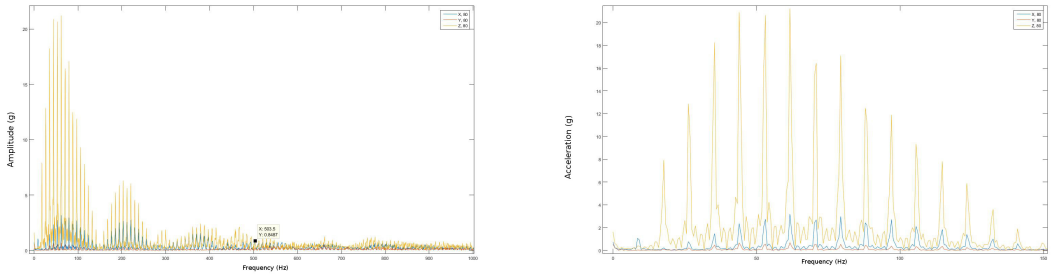

Figure 4: Most of the energy is found in 10-100 Hz range.

where ω is the rotation speed of tyre and r is the radius of rotation.

2.3 Energy harvesting

2.3.1 Overview of methods

First step of designing a system for energy harvesting was to identify the currently known methods and their properties. Kubba et al. [23] have done a study on tyre pressure sensor technology, they present electromagnetic, electrostatic, piezoelectric and thermal solutions as possible candidates for energy harvesting. In addition, triboelectric and magnetostrictive methods have been proposed by Bowen et al [10]. Outside of the context of tyres, Paradiso et al. [34] present solar and radiowave harvesting techniques. Radioactive power source has been suggested by Lal et al [24].

Electromagnetic power sources are based on Faraday's law of electromagnetic induction. A magnet and a coil are put in motion relative to each other, and the changing magnetic flux through the coils of the generator produces voltage. Current through such device is determined by load resistance. Technology is widely used in power generation, where a primary power source such as wind or flow of water provides

rotation for the generator. While conventional designs use rotational movement, linear generator designs exist. Boldea and Nasar [7] provide an overview of linear generator and actuator theory.

Electrostatic devices charge plates of a capacitor and use mechanical vibration to vary the structure of the capacitor. As the capacitance value changes with the structure, energy can be harvested from increased potential energy in capacitor. Drawback of this method is the required control electronics and high polarisation voltages needed for maximal efficiency. There are also electrostatic methods which use electrets. These electrets hold constant charge and polarisation for years and they can be used in electrostatic harvesters which do not require an external excitation source [6]. As electret elements and electrostatic generators are not readily available, they have been excluded from this study.

Piezoelectric materials generate charge in response of mechanical stress. This stress can be caused by firmly attaching the piezoelectric element to a surface which deforms (simply supported) or by leaving one end of the element free-hanging while other end is fixed (cantilevered). Dynamics of the generator are very different for the different configurations, Kim et al. [22] provides a model for impact-based piezoelectric harvester while Erturk et al. have done in-depth analysis of cantilevered piezoelectric modelling [13].

Thermal solutions can be further divided into subcategories. Seebeck-effect where a temperature gradient in a semiconductor material causes voltage between poles of the material is widely used in temperature sensing, but to generate appreciable amounts of power large temperature gradients of over hundred °C are required according to study by Amatya et al. [1]. Such temperature gradients are not practical inside the tyre. Pyroelectric materials do not require differential of temperature, they generate energy when the temperature of the entire element changes [45]. As the temperature inside tyre remains rather constant over long periods of time, these methods are not practical for this application.

Triboelectricity generates power using friction between two materials, a classic example of this is Benjamin Franklin's experiments on charging various rods by rubbing them against different materials. A flexible triboelectric generator has been presented by Fan et al. [15]. Triboelectric sheets are not readily available and their construction is complex, so triboelectric generation is excluded from this work.

Magnetostrictive materials change their magnetic field in response to external mechanical stress. This change can be utilised to create a magnetic flux through coils as in electromagnetic generators. A magnetostrictive generator was built by Wang et al. [43].

Solar energy can be harvested by using sun as a energy source for a thermal energy harvesting or by utilising the photovoltaic (PV) effect to generate electricity from photons hitting PV material. PV technology is mature and widely used, and PV cells attached to rim of tyre could produce ample power during summertime. PV cells would however incur extra maintenance as the rims would have to be cleaned whenever power output falls.

Radio wave harvesting uses antennas to collect energy from ambient radio transmissions, such as WiFi- and cellular signals. Patel et al [35] have built a demonstration

device which uses TV broadcasts as an energy source. The tyre material dampens any Radio frequency (RF) broadcasts, which makes RF energy harvesting poorly suited for the application.

Radioactive energy harvesting resembles battery or fuel cell. A radioactive material is deposited in generator near piezoelectric cantilever. Radioactive decay charges proof mass of piezoelectric cantilever until the proof mass contacts the radioactive material by electrostatic attraction, at which point the electrical charge is balanced and piezoelectric beam begins resonant vibration as in normal piezoelectric harvesting. Such a battery has lifetime limited only by half-life of the used material. Lal and Blanchard [24] present such a battery. This kind of battery would be redundant for the application, as there already exists energy in rotation of tyre which can be used to energise the cantilever.

In conclusion, a wide range of energy harvesting technologies have been identified. As their primary properties are known, we can narrow down the suitable technology to electromagnetic, piezoelectric and magnetostrictive. These technologies are studied further to identify optimal choice for the application.

2.3.2 Resonance-based piezoelectric harvesting

Piezoelectric materials produce voltage in response to mechanical stress. The effect is bidirectional, piezoelectric element can also produce mechanical strain in response to applied voltage. The material has crystalline structure with electrical dipoles in balanced state when no stress is applied. Mechanical stress unbalances these dipoles, creating element which electronically resembles a charged capacitor.

A common approach to piezoelectric harvesting is to configure the element as a cantilever and tune the resonant frequency of the system to dominant frequency of the surrounding environment. This kind of system is shown in figure 5. In some applications, such as in machines running at the frequency of power grid (50 Hz or 60 Hz) this kind of frequency-tuning is relatively straightforward.

Figure 5: Piezoelectric generator configured as cantilever by Arroyo et al [3].

This kind of resonant harvesting is challenging in tyre. The energy harvester has a very sharp peak efficiency frequencies, and dominant frequency of tyre varies with the speed of car. On the other hand, there is almost guaranteed broadband energy available from moments where tyre contacts road. There is also some research

on tuning the resonant frequency of cantilevered piezoelectric harvester by Singh et al [39]. They used intelligently driven SMPS to impedance-match the load to piezoelectric element. As the electro-mechanical nature of piezo means changing load changes the mechanical properties of element, resonance frequency can track the dominant frequency of system within some limits. Figure 6 shows the tracking behaviour Singh et al achieved, resonance can be adjusted in range of 65 - 70 Hz.

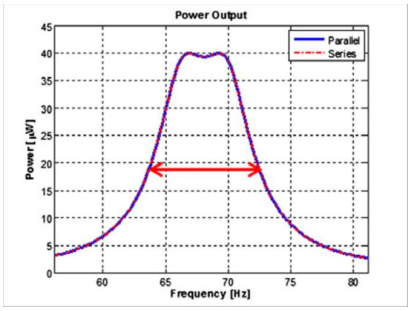

Figure 6: Frequency tuning results by Singh et al [39].

The results of Singh et al. can be considered as the state-of-art for resonance-based piezoelectric harvesting in tyre, and their power output was around $40\mu W$ at peak efficiency. Therefore other methods have to be explored for energy harvester design.

2.3.3 Impact-based piezoelectric harvesting

As the resonant harvesting is not feasible in the environment inside tyre, another method would be to use an impactor to hit a piezoelectric plate on every cycle of a tyre. These impacts would provide energy once per rotation of a tyre. This method has been tried before by Manla et al [27]. Their generator produced 4 mW electrical power.

As 4mW is plenty in field of low-power electronics, this approach deserves an in-depth study. Thunder TH-5C piezos have been used in previous studies of piezoelectric harvesting and they have produced promising results, so they were selected as the piezoelectric element for this thesis.

Piezoelectric elements are often electrically modelled as current source with parallel capacitor or voltage source with series capacitor, as shown in figure 7 by Kanda et al [21]. There are also a lot more complex models which account for mechanical phenomena in piezo, as well as loading effects coupling on mechanical model. For the purposes of model identification for the piezo only simplest voltage source (a) and current source (b) models are explored.

Series of tests were ran to determine characteristics of piezoelectric power generation under impacts. Mossi et al [31] have produced a recommended test process for Thunder piezoelectric actuators shown in figure 8.

This setup was replicated using a solenoid actuator as impact force generator, precision scale as load cell to measure impact force and oscilloscope to view output waveforms. An eraser was cut to shape to act as preload bellow to spread the impact

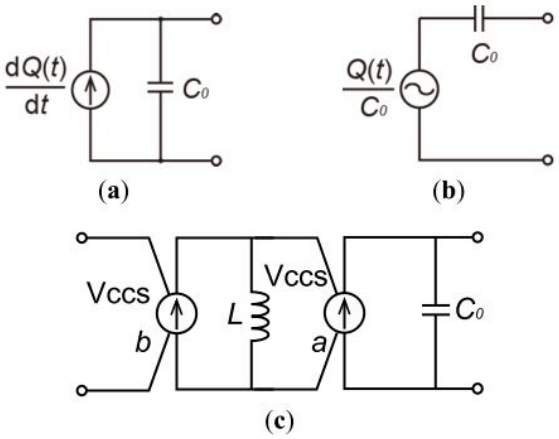

Figure 7: Electrical equivalent models for piezoelectric element [21].

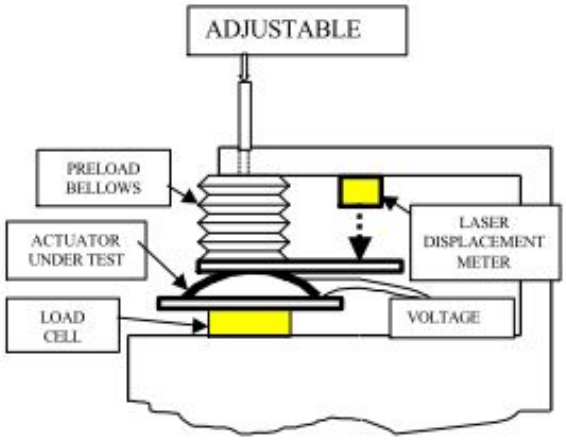

Figure 8: Recommended evaluation platform for Thunder piezos [31].

over larger surface area of piezo, displacement was not measured. The test setup is shown in figure 9. An electronics prototyping platform, "breadboard", was used to house test electronics including resistive ladder and Arduino to trigger the solenoid at adjustable duty cycles. Load force was controlled by setting the stroke length of solenoid shaft and fine tuned by adjusting voltage over solenoid.

The measurement results are shown in figure 10. Output voltage scales with square of impact force, which makes sense as work done can be expressed as $W = F * d$, where W is work, F is force and d is distance force acts on object. As the displacement of piezo grows with the applied force, total work and therefore energy grows with both terms.

Peak voltage grows with the load resistance. This makes sense in both voltage source and current source models, as the capacitor starts to discharge through load resistance instantly when voltage is applied over it. The relationship between voltage

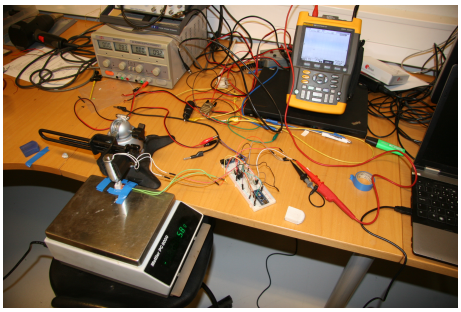

Figure 9: Test platform for piezo characteristics.

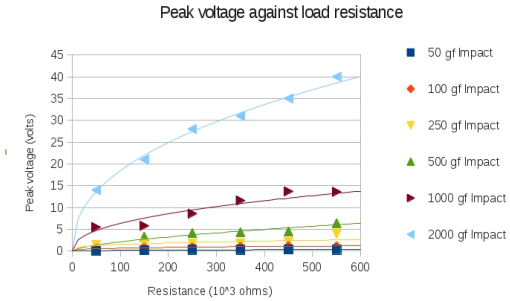

Figure 10: Measured output voltage at different loads and impact forces.

and load resistance seems to be logarithmic, which would be in good agreement with the logarithmic discharge curve of capacitor-resistor system. Peak voltages were read out from digital display and they can be considered reasonably accurate.

The time constants for voltage halving was graphically measured from oscilloscope waveforms, and this data was used to calculate the capacitance of TH-5C. These measurements are a lot less accurate, as readouts from oscilloscope screen have resolution of approximately half of line division, leaving accuracy of measurements at $\pm 2.5ms$. These results are plotted in figure 11

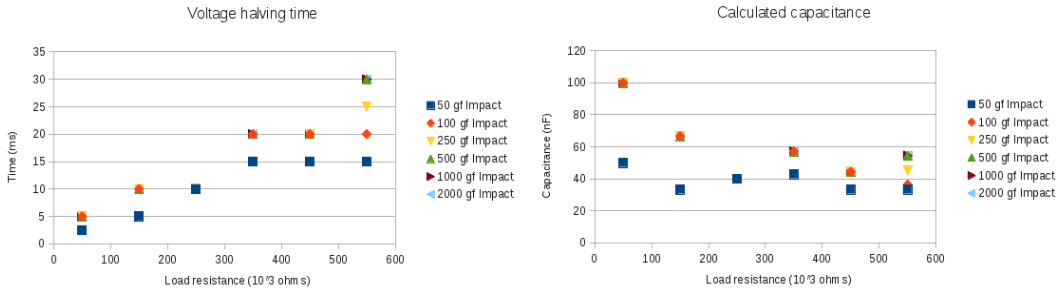

Figure 11: Measured half-time of system and calculated capacitance of piezo.

The half-time data can be used to calculate capacitance of piezo using the RC-time

constant of circuit:

$$C = \frac{t}{-ln(\frac{1}{2})R} \tag{2}$$

TH-5C provides value of 39nF as the capacitance, while these calculated values are notably higher and rise with the loading of piezo. Most likely explanation of this observation is the mechanical response time of system: solenoid plunger will take some milliseconds to reach new force equilibrium, and this effect becomes more pronounced at smaller time constants of RC-system. Using the known voltage and capacitance energy and peak power in impact can be determined:

$$E = \frac{1}{2}V^2C \tag{3}$$

$$P_[peak = \frac{V^2}{R} \tag{4}$$

The calculations are plotted in graph 12. As these calculations are based on inaccurately measured time, they should not be used as reference for any further calculations. However, trends can be seen in these values.

Interestingly the peak work done by piezo to resistor seems to be almost constant on all load levels. This is probably a consequence of logarithmic voltage-load relationship described above. There is a possibly significant result based on these findings: total energy obtainable from harvester grows with load resistance. However, this is applicable only for resistive load under impact-based energy generation.

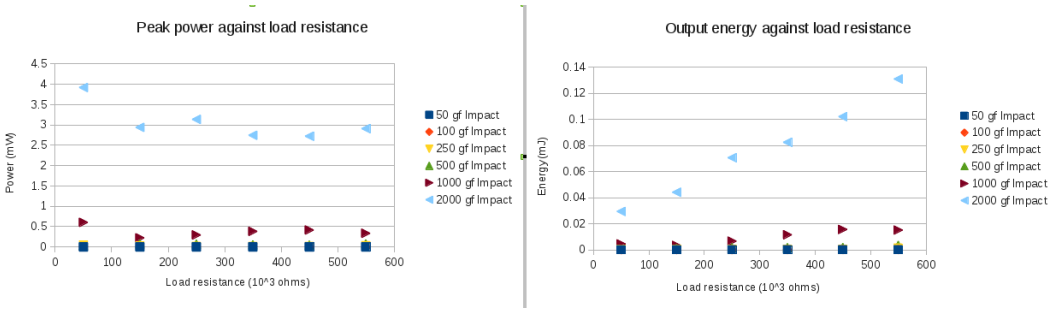

Figure 12: Calculated piezo power and energy output

Based on these results, an electrical equivalent model of circuit was designed. The model is shown in figure 13. Model has two parallel current sources, one to simulate impact of plunger on piezo and other to simulate release of the impact. Capacitance in parallel is set to 39 nF as given in datasheet, load resistance is parametrised to step through the experimental values.

Model was tuned by first calculating the total current transfer to reach the open circuit voltage over capacitor. Then maximum current of current sources was matched to reach peak voltage over highest load. The simulated data is plotted figure 14.

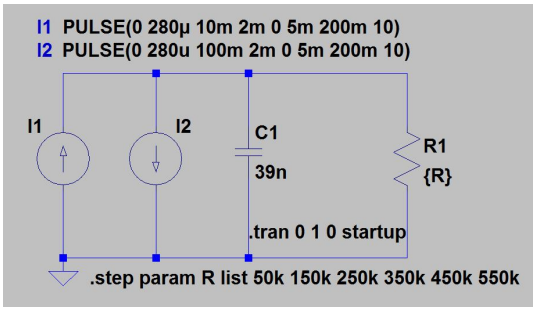

Figure 13: Equivalent model of piezo in LTSpice simulator

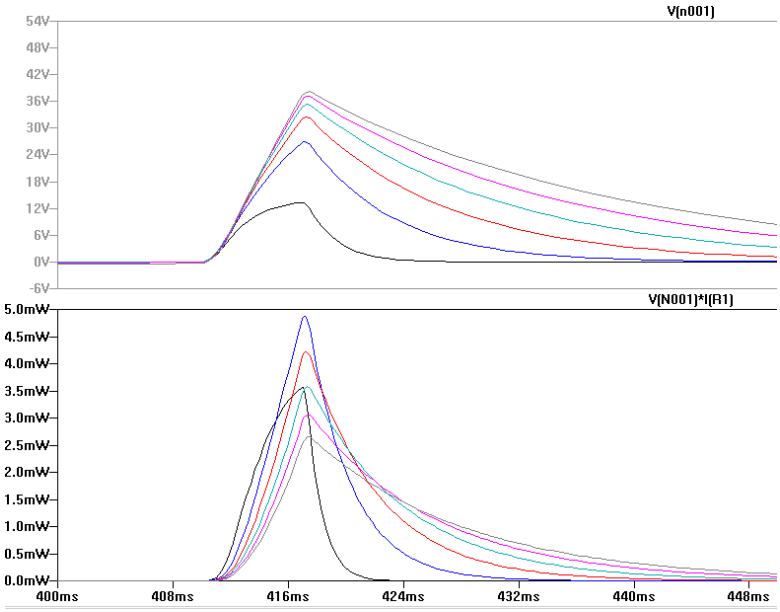

Figure 14: Simulated piezoelement output voltage and power waveforms. Loads are stepped through list to match experimental values at 2000 gf impact force. Black: 50k; Blue: 150k; Red: 250k; Turquoise: 350k; Violet: 450k; Gray: 550k

The experimental and simulated data are not in a good agreement. While maximum and minimum load voltage and power are close to estimated values, this is by design as model is tuned to these measurements. Problems occur in interpolating the results, as output voltages are notably higher than measured values. This provides a result which sets the maximum power load near the value which provides output voltage of half of the open loop voltage. This is especially interesting as LTC3331 datasheet [**?**] suggests to set the circuit to track the load at this same half-point of open loop voltage. Both LTC3331 and LTSpice are made by Linear Technology, so independent verification of this result would be needed.

2.3.4 Electromagnetic harvesting

Electromagnetic harvesting is based on Faraday's law of induction: A loop of wire acquires electromotive force (EMF) in response to a changing magnetic field. More formally:

$$\varepsilon = -\frac{d\Phi_B}{dt}, \tag{5}$$

where ε is the EMF, Φ_B is magnetic flux through loop area, and t is time. Negative sign signifies that emf opposes the change of magnetic flux. For a tightly wound coil of wire, the equation can be stated as:

$$\varepsilon = -N_{turns}\frac{d\Phi_B}{dt}, \tag{6}$$

where N_{turns} is the number of turns in a coil. [44, p.999]

It's important to notice that magnetic flux through wire Φ_B can change for a variety of reasons: the source of field can be in motion, strength of field can vary, the coil can be in motion, and the shape of coil can vary. In an energy harvesting application in an environment with vibrations motional energy is readily available, so we focus on energy harvesting methods which either move the source of magnetic field or the coil itself.

It can be determined from equation (6) that the energy available increases with the strength of magnetic source, number of turns in a coil and rate of change in the magnetic field.

Magnetic source can be either a permanent magnet or an electrically induced source as in induction motors. Induction-based generators require reactive power to start up, which means that any harvester design incorporating an induction generator would need a secondary power source to start the inductive generator. Hence the focus of this thesis will be in permanent magnet designs.

In addition to voltage available from the generator, it's important to consider the source impedance. A very simple electrical equivalent model of the generator is presented in figure 15, where generator is presented as a voltage source in series with lumped inductor and resistor [20].

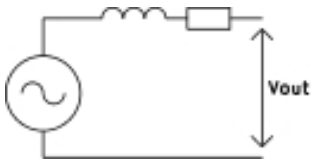

Figure 15: A simple electromechanical generator equivalent circuit.

.

This model is greatly simplified and it does not account for factors such as effect of electromagnetic force on mechanical structure of the generator. Even with these limitations, the model is still useful as it can be used to determine an optimal load for the generator.

The power output can be written formally as:

$$P_{generated}(s) = \varepsilon(s) * I_{generated}(s), \tag{7}$$

where $P_{generated}(s), \varepsilon(s), I_{generated}(s)$ are complex frequency-domain power, voltage and current dependent. Voltage is determined by EMF as described above. Current can be written as:

$$I_{generated}(s) = \frac{\varepsilon(s)}{Z_{generator}(s) + Z_{load}(s)}, \tag{8}$$

where $Z_{generator}(s)$ and $Z_{load}(s)$ are complex impedances of load and generator. This equation is valid only for linear systems, so for example rectifying and converting power with switch-mode power supply (SMPS) reduces accuracy of the equation. Substituting (8) into (7) we obtain:

$$P_{generated}(s) = \varepsilon(s) * \frac{\varepsilon(s)}{Z_{generator}(s) + Z_{load}(s)}. \tag{9}$$

Total power into load can be written as:

$$P_{load}(s) = \varepsilon(s) * \frac{Z_{load}(s)}{Z_{generator}(s) + Z_{load}(s)} * \frac{\varepsilon(s)}{Z_{generator}(s) + Z_{load}(s)}. \tag{10}$$

It's easy to see from (10) that if the load impedance is infinite or zero, there is no power generated. It can be shown that maximum power is generated when load impedance is complex conjugate of generator impedance, $Z_{generator}(s) = Z_{load}(s)^*$. Another consideration is efficiency of the generator: the electrical efficiency is defined as ratio of power flowing into load and total power generated. Equation (10) can be used to show that when load impedance is equal to generator impedance, efficiency is 50%. Efficiency rises with the load impedance, which is why generators are rarely run at their maximum power. In our application the harvested power is minuscule compared to power available in tyre, so it makes sense to try to match the load impedance for maximum power.

In an energy harvesting application it is important to consider the validity of established theory when generator is scaled to centimetres or even smaller dimensions. Many assumptions, such as coil being tightly wound and made of thin wire might become invalid at microscale. O'Donnel et al. [33] have done a study on the effects of scaling dimensions downwards down to millimetre range, and they concluded that power available from generator is proportional to fourth power of generator dimension for cubical generators. Another of their primary findings was that a microfabricated generator becomes more effective than a traditional wire-wound generator when design is scaled below $2mm$ length or in $8mm^3$ volume. It can be concluded that in this application it is reasonable to use a wire-wound generator over microfabricated one, as the generator dimensions can be an order of magnitude larger than this crossover point.

3 Design

3.1 System-level design

The complete system will consist of energy harvesting source, energy storage for times when harvested energy is not available, AC/DC and DC/DC converters for maintaining required voltage levels in different blocks of system, accelerometer for measuring the accleration in tyre and radio/microcontroller module for transmitting data from acceleromoter. Figure 16 shows the power and data flow between subsections of system.

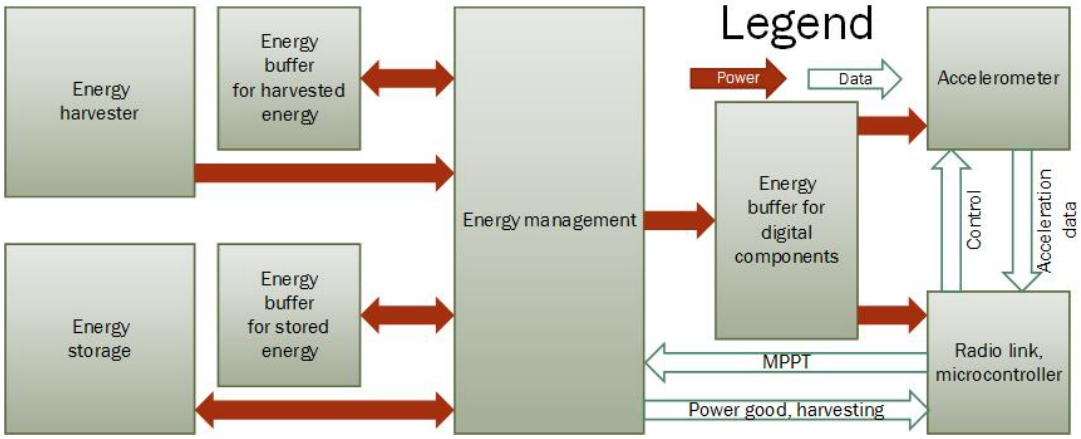

Figure 16: Block diagram of complete system.

Energy harvester can be any suitable source for electrical energy. Energy management section rectifies AC voltage and buffers the rectified voltage on a capacitor. The energy storage can be a supercapacitor or rechargeable battery. Both of these storage technologies can benefit from having a low equivalent series resistance (ESR) capacitor in parallel to supply any sudden peak currents. Energy management circuitry chooses whether to use harvested energy or stored energy and regulates the energy to voltage level compatible with the system. Digital components require their own local power buffer capacitors to supply high-frequency currents required by megahertz clocks onboard these circuits.

Microcontroller is used to manage the application layer of system. For example the microcontroller can send status updates over radiolink more often if there is harvested energy available and reduce system power consumption when system is running on stored energy.

Next section presents details of expected power consumption and duty cycles for various components. A few components are selected to provide examples of suitable system power.

3.2 Power requirements of a system

The sensor system will be in three distinct states. One is sleeping, conserving power as much as possible while car is not moving. Second state is measuring, when the radio connection is off but electronics are active and gathering data. Third state is transmitting, when the data is relayed to drive computer in car.

Energy and power consumption are estimated by reviewing a few suitable components and their power requirements. Energy management is handled by a specialised integrated circuit (IC), for example LTC3331 [40].

Communication is handled by a Bluetooth-low energy (BLE) module, which contains a general-purpose microcontroller for application flow control. We use BLE113 [5] as an example of such module.

Finally there is an accelerometer which is used for gathering data out of the system, ADXL375 [38] is used as an example. ADXL is a low-power digital accelerometer with dynamic range of 200g. Table 1 summarises the estimated power requirement of each subsection of system. System level voltage is selected to be 2.5 V, as that is lowest voltage which LTC3331 can supply and allows all devices to function. Lowest possible voltage is selected to reduce the power draw.

Table 1: Current and power consumption of system at different activity levels.

Device	**Sleep**	**Monitoring**	**Communicating**
LTC3331	0.2 μA	80 μA	16 250 μA
BLE113	0.9 μA	275 μA	26 000 μA
ADXL375	0.1 μA	140 μA	140 μA
Total power	3 μW	1 200 μW	110 000 μW

Current consumption levels for BLE113 and ADXL375 are taken from the datasheets of the components. Battery manager power draw is estimated by calculating required power to supply the rest of the circuit at 80 % efficiency. Power consumption is calculated from current draw with assumption that system voltage will be constant $2.5V$.

Power consumption grows by orders of magnitude when the activity is stepped up to the next level. Therefore it is important to keep the system in sleep whenever possible, for example when the car is parked and wake up only periodically to check if movement has started. Monitoring starts once car is moving, and device will send brief pulses over the radio link when necessary.

When the power consumption is compared to values achieved in previous studies of energy harvesting, it can be seen that sleep current can be compensated by a reasonable harvester design. Powering constant monitoring would be a greater challenge, but with realm of feasibility. Providing power for continuous radio transmissions is not feasible even with current state-of-the-art harvester designs.

Next sections detail designs and preliminary analysis of electromagnetic generator designs. The initial designs are then evaluated based on their ability to supply

required power levels to circuitry.

3.3 Electromagnetic harvester design

3.3.1 Basics of electromagnetical vibration harvester

Electromagnetic harvesters utilise vibration to move a magnet inside a coil. The movement of a magnet causes a changing magnetic field, which gets coupled to a coil. The coil opposes the change in magnetic field by inducing electrical current in the device. A device could be built with a spring-loaded magnet to balance out the static acceleration of a tyre, an added benefit to spring loaded mechanism would be the utilisation of resonant frequency of the spring-mass system: as the system gets a shock, some of the energy would be in correct frequency range to make the magnet oscillate inside coil allowing generation of energy until next shock. The coil will also function as a damper to system, so no extra damping is required. Modern neodymium magnets do not lose their magnetization by vibration, so long magnet can be reliable for a long time period.

A theoretical design of linear generator (LG) was made. Most common generator designs use a rotating magnet inside coils to generate alternating current. As the mechanical apparatus for converting the linear accelerations inside the tyre to rotational movement would add to complexity and cost of the tyre, generator is designed to use the linear motion as the power source.

Basic principle of operation of LG is similar to traditional rotational generator. A moving magnet creates alternating magnetic field which is coupled to coiled conductors. The conductors oppose this change of magnetic field by inducing an electrical current across their ends. The design can have multiple phases and poles, where phases refer to parallelly connected coils and poles refer to serially connected coils. Multiple phase designs can have lower resistive losses in wiring, as the resistive losses are propotional to square of the current. However paralleling phases requires separate rectification for each phase, which leads to increased rectification losses. Adding poles to design increases the output voltage and frequency, but having a small airgap between the coils and magnets becomes critical to maintain efficiency of the generator [11].

Energy harvester designs sometimes use several poles to increase the frequency of the power output. This increased frequency allows to use smaller energy storage components such as capacitors to keep the device powered until next cycle. The characteristics of the tyre make this point irrelevant, as energy is available once per revolution of the tire when generator contacts the ground and when the contact ends. Any energy storage device has to maintain power until the next cycle, and no increase of the frequency while generator is in contact can alleviate that. Therefore number of poles is minimized to reduce complexity. Pole number is selected as two, so there is one negative and one positive pole. Mechanical design can utilise resonant vibration to function as energy storage device instead of electrical or electronic storage.

First design decision was whether to use a moving magnet or moving coil type of a design. Moving coil designs tend to have lighter moving parts which is a very

important feature in high-power designs where mass of the generator is large. On the other hand, moving coils require flying leads [19], which is a long-term reliability concern [7]. Boldea and Nasar [8, p. 203] conclude that moving coil designs aren't practically interesting, so the design is focused on moving magnet generator.

A rough model for designing initial prototypes was done previously by Elmes [12]. As the work verified the model experimentally and found the model to be reasonably accurate, it was adapted to form basis of linear generator model. The model can account for most of the key design parameters.

There are two different approaches to generator structure. One is magnets inside, and coils on the outer rim of the generator. Other is to use ring magnets on the outer rim and have the coils on the inside. Both methods have their advantages: Having magnets on the outside allows larger and therefore stronger magnets and creates horizontal support for the magnets as they move along the shaft. Having coils on the outside increases wiring radius which results in greater power if other parameters are held equal. In-depth study of both concepts is done to select optimal structure for generator.

The height of the generator is constrained at 45 mm to avoid contact between tyre rim and generator. Initially the height of the generator was selected to be 35-40 mm to leave some margin while still being as tall as possible. Lower weight is desirable to avoid unbalancing the tyre, but there is no specific absolute maximum mass for the device.

A method to counter the centripetal acceleration is needed to keep the magnet on the centre of the generator. Ideally, such method would always balance the magnet in the middle of generator against any external constant force, but active control is not achievable without adding to complexity and power consumption of the generator itself. Passive negative feedback method has to be used instead.

Springs are often chosen to balance the magnets, but as the centripetal acceleration grows exponentially with the speed of the car, any linear spring would be usable only for very limited range of speeds. Non-linear conical springs which have the added benefit of compressing into very small height are available.

Another approach would be to use two additional magnets fixed to top and bottom of the generator in repulsive configuration. Force between magnets is inversely propotional to fourth power of the distance [2], which leads to a strong negative feedback on the position of the magnet. Tornincasa et al. [42] proposed one such design, shown in figure 17.

Figure 17: A magnetically balanced linear generator by Tornincasa et al. [42]

.

Magnetic floating is an attaractive solution, as magnets can be thin and they do not wear out with aging. On the other hand, any imbalance in the magnets result in torgue which causes increased friction. 18 This issue is further aggravated in designs where shape of the generator shaft is not a smooth cylinder. Therefore the

design should have reasonably smooth and low-friction material on the inner shaft to minimize losses.

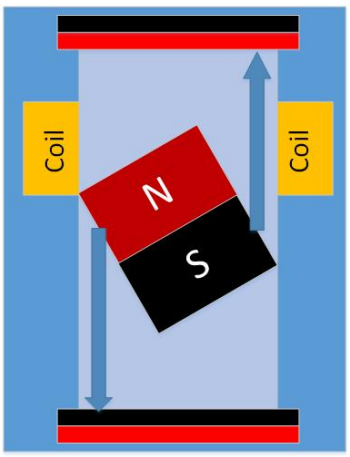

Figure 18: Angle in magnet causes torgue which results in increased friction

.

3.3.2 Analytical model of electromagnetical vibration harvester

A common starting point for analysis of linear generator is to model the mechanical domain as Mass-Spring-Dampener system decipted in figure 19. A mass "floats" in system, a spring balances the mass towards centre and a damper represents frictional forces opposing any movement of mass.

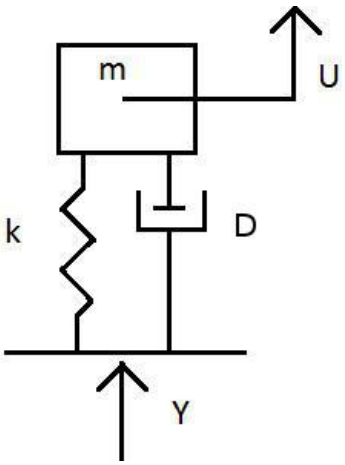

Figure 19: Mass-spring-damper system.

Input Y is the force applied to the base of system, output U is the position of mass block relative to "zero". Zero is usually set to point where mass settles when no input, including gravity, is applied to system. Paramters m, D, and k are mass,

damping constant and spring constant of system, respectively. Input-output-equation in time domain can be written as:

$$m * \ddot{U}(t) + D * \dot{U}(t) + k * U(t) = Y(t). \tag{11}$$

As the force $Y(t)$ is defined as $Y(t) = m * a(t)$, and the acceleration $a(t)$ can be considered constant regardless of any reasonable mass m of system, equation (11) can be written as:

$$\ddot{U}(t) + \frac{D * \dot{U}(t)}{m} + \frac{k * U(t)}{m} = a(t). \tag{12}$$

This form is convenient for analysis, as the acceleration measurements from previous research are available and they represent real-world values. Mass m can be considered constant, as the system does not exchange matter with surrounding environment. As magnetic suspension was selected, the paramter k cannot be considered as a constant, but rather a function of mass position $k(U)$. Centripetal force can be considered as a constant DC-component of function $Y(t)$, and is not included in analysis of function $k(U)$. According to D. Amrani [2] force between two magnets can be approximated as

$$F(x) = \frac{3\mu_0 m_1 m_2}{2\pi} * \frac{1}{x^4}, \tag{13}$$

where $F(x)$ is force as a function of distance x between magnets, μ_0 is the permeability of vacuum, m_1 and m_2 are magnetic dipole moments of magnets under examination. This equation is only valid when x » h, where h is thickness of the magnet. As two magnets are used to suspend the rotor magnet, total force acting on mass becomes

$$F(x) = \frac{3\mu_0 m_r m_l}{2\pi} * \frac{1}{(x_0 + x)^4} - \frac{3\mu_0 m_r m_u}{2\pi} * \frac{1}{(x_0 - x)^4}, \tag{14}$$

where m_l, m_u, m_r are magnetic dipole moments of lower suspending magnet, upper suspending magnet, and rotor magnet. x_0 is the distance to middle point of generator and x is the displacement of rotor magnet from aforementioned middle point, positive direction being upwards. Figure 20 shows the system.

Regrettably, the expression (14) is very inaccurate for magnets where diameter is large compared to thickness of magnet, and the problems are compounded when distance between magnets is small. Therefore final design should be optimized using measurement data or finite element analysis (FEA) for determining $k(U)$.

Damping parameter D is likevise a function electromagnetic force acting on magnet, friction between magnet and stator and pneumatic damping caused by compression of air in generator. Tornincasa et al. [42] divided this damping parameter into three distinct terms to account for these different physical phenomena in damping. Let us call them $D_{emf}, D_{friction}$, and D_{air}, respectively. D_{emf} represents power extracted from the system into electrical current, it can be written as:

$$D_{emf} = BIlsin(\phi), \tag{15}$$

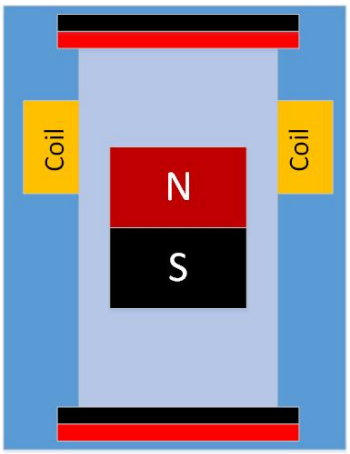

Figure 20: Linear generator with rotor magnet balanced by endstop magnets

.

where B is magnetic field affecting coil (presumed constant), I is current through wire depending on load and generator properties, l is total length of wire in coil and ϕ is angle between coil and magnetic field, presumed to be 90 °. Assuming the load impedance is the complex conjugate of coil impedance for maximum power harvesting, we can substitute the I with equations (6) and (8), which results in:

$$D_{emf} = B\frac{\varepsilon}{2 * Re(Z_{generator})}lsin(90°), \tag{16}$$

where $Z_{generator}$ is the impedance of generator. As the load impedance is complex conjugate of generator impedance, their series connection has only real (purely resistive) component. This assumption fails on real-world application with non-linear rectification and DC/DC conversion, but it can be used as a basis for analytical examination of the generator. As ε can be substituted with (6), we obtain:

$$D_{emf} = B\frac{-N\frac{d\Phi_B}{dt}}{2 * Re(Z_{generator})}lsin(90°), \tag{17}$$

The relationship between $N\Phi_B$ and $Re(Z_{generator})$ can be further studied by writing

$$\Phi_B = \iint_{\Sigma(t)} B(r,t)\, dA, \tag{18}$$

where $\iint_{\Sigma(t)}$ signifies possibility of loop area changing over time and dA is element of surface area. If we assume the coil to be a perfect tightly wound circle which does not deform over time, we can write the relationship between number of turns in coil, area of coil, and resistance of coil as:

$$R = N2\pi A\rho_{wire}, \tag{19}$$

where ρ_{wire} is resistivity of coil wire. Substituting (19) and (18) into (17) we finally obtain reasonably accurate expression for D_{emf} which accounts for all the design parameters affecting it:

$$D_{emf} = B\frac{-N\frac{d[\int\int B(r,t)\,dA]}{dt}}{2 * N2\pi A\rho_{wire}}lsin(90°). \tag{20}$$

A few observations can be made from this equation: first, the magnetic field strength B and it's derivate in respect to time increase the D_{emf} which signifies the electrically extracted useful power. Therefore it makes sense to use as strong magnets as possible, as long as other parameters aren't adversely affected. Second, both the number of turns and the loop area are as multipliers and divisors, which means they should be optimized to find best applicable values. Third, resistivity of wire limits power that can be extracted, so intuition would lead to minimizing wire resistance. In practise the wire resistivity can be decreased by increasing wire diameter, which in turn leads to lesser number of turns in same volume and mass of coil. Therefore, also wire diameter and material should be optimized to find desirable compromise in generator design.

Next we examine $D_{friction}$ in detail. Friction is modelled as Couloumb fricion:

$$F_s = \mu_s N, F_k = \mu_k N, \tag{21}$$

where F_s and F_k are static and kinetic friction forces opposing movement, μ_s and μ_k are friction coefficients in static and kinetic situations and N is normal force along X- or Y- axis. Normal forces are estimated by using existing acceleration data and calculated mass of magnet. Coefficients of friction are looked up from supplier of stator material. Transfer between static and kinetic models is assumed to be a step, if velocity of magnet is 0 along Z-axis, μ_s is used, μ_k othervise.

Finally, there is pneumatic damping of the system, D_{air}. In a closed tube, the central magnet can be thought as a piston dividing generator into two chambers. If there is insignificant airflow between chambers, any force caused by pressure deltas between chambers act as a spring. However, some airflow is to be expected due to clearance between magnet and stator. Tornincasa et al. [42] modelled this effect by adding a virtual centrepoint for pneumatic spring, this centre moves through a virtual damper which models the airflow between chambers. End result is that pneumatic spring takes some energy from movement, and this energy stored into pneumatic spring is dissipated as the centre moves until potential energy stored in the spring is zero.

The force from pressure differential is:

$$F_{\delta p} = \frac{\pi d^2}{4}(p_{lower} - p_{upper}), \tag{22}$$

where d is diameter of magnet and $p_{lower} - p_{upper}$ are pressures in chambers. Pressures can be estimated from ideal gas law:

$$pV = NRT \tag{23}$$

where p is pressure, V is volume, N is amount, R is ideal gas constant and T is temperature. Temperature is assumed to be constant. Initial pressure is assumed to be same as tyre pressure and magnet is assumed to be exactly in midpoint at start. Change of volume can be calculated from change of height caused by movement of the magnet.

Mass flow between sections can be estimated with equation given by Fox et al. [16]:

$$\dot{m}_{1\to 2} = \frac{\rho\pi d\delta_{r^3}}{12\mu h}(p_1 - p_2), \tag{24}$$

where ρ is air density, δ_r is radial clearance, μ is dynamic viscosity and h is the height of magnet. [42]

There is also frictional dissipative force as the air passes along the edges of the cylinder. This frictional force has magnitude of:

$$F = \mu * \rho * \frac{\pi dh\dot{z}}{\delta}[29]. \tag{25}$$

Analytical expressions for the equations governing the mechanical movement of magnet inside generator have now been identified. Some of the non-linear functions are hard to solve analytically, therefore experimental or FEA methods should be used for creating approximations for these functions.

The analytical effect of these parameters is summarized in table 2

Table 2: Effect of parameters of generator

Parameter	**Increasing**	**Decreasing**
N_{turns}	Higher voltage	Smaller size, less wiring resistance
N_{pole}	Increased frequency	Decreased frequency
l_{pole}	More space for wiring	Higher voltage, smaller size
A_{loop}	More power	Smaller length of wiring
B	Increased power	Smaller magnets
r_{wire}	Decreased wiring resistance	More turns in same space
δ_r	Stronger side walls	Incresed efficiency

3.3.3 Experimental and FEA modeling of electromagnetic harvester

As some parameters of the harvester are difficult to solve analytically, these parameters are solved using experimental and FEA methods. First one of these difficult interactions is the magnetic force between rotor magnet and balancing magnets. A magnetics FEA software FEMM [30] was used to create an axisymmetric model of magnets in generator. Figure 21 shows the used model. Model has two biasing magnets made of N40-neodymium alloy configured to repel an identical rotor magnet.

Magnets have height of 2.5 mm and diameter of 11 mm, walls of generator are modelled as air. Generator has total height of 25 mm, leaving rotor magnet 17.5 mm room for movement inside generator.

Weighted stress tensor integration over rotor magnet volume as implemented by FEMM was used to determine FEA value for net magnetic force acting on rotor magnet. A LUA script was used to move the rotor magnet from bottom of the generator to top in 0.1 mm increments and values obtained from analysis were exported as CSV data for plotting in a spreadsheet software as well as to create a lookup-table for MATLAB/SIMULINK simulation. Figure 21 shows the force on magnet, positive force meaning force towards the upper magnet and zero height being at the bottom of cylinder. For reference the centrifugal force acting on magnet was also calculated at various speeds, assuming weight of the magnet is 1,67 g and radius to bottom of generator is 275 mm.

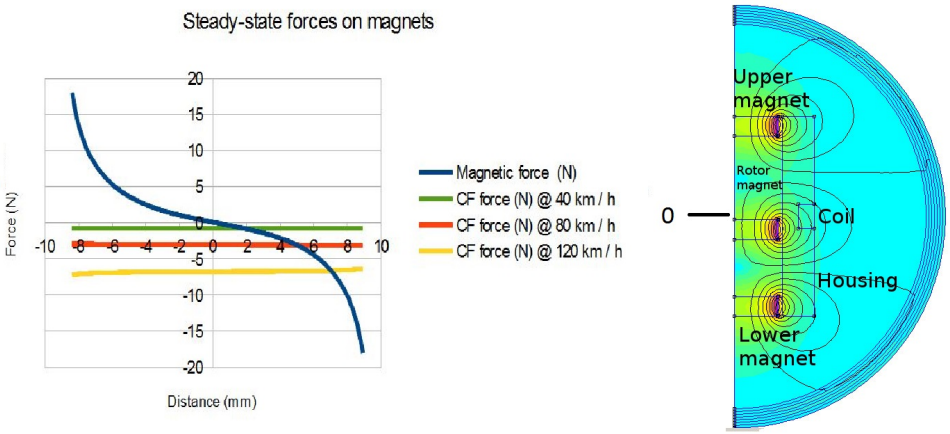

Figure 21: Steady-state forces acting on magnet

It can be seen that net force on rotor magnet is dominated by the magnetic forces at lower speeds. Centrifugal force on magnet becomes significant at higher speeds, but even at 120 km/h speed the rotor magnet will stay clear of the bottom. Second use for this FEA analysis is to create look-up table for flux linkage into coils of generator. The methodology was similar to determining forces affecting the rotor magnet: a LUA script was ran to sweep possible magnet positions, and look-up table of flux linkage into coils was created. For the purposes of analysis, difference of flux linkage was calculated between each point. The change of flux linkage is a very important parameter, as the power generated is proportional to $\frac{d\Phi_B}{dt}$.

Based on these results, a magnet moving at the speed of $0.1mm/s$ would induce voltage of up to $1.5mV$ in each winding of the coil. If we assume coil to have 100 turns, travel length of the magnet to be 1 mm, and frequency of magnet moving inside generator to be 10 Hz the peak voltage out of generator would be sufficient to power the circuitry and charge battery of sensor.

A prototype generator was built to test the concept feasibility and identify any practical issues in the generator construction. Generator was machined out of 21mm

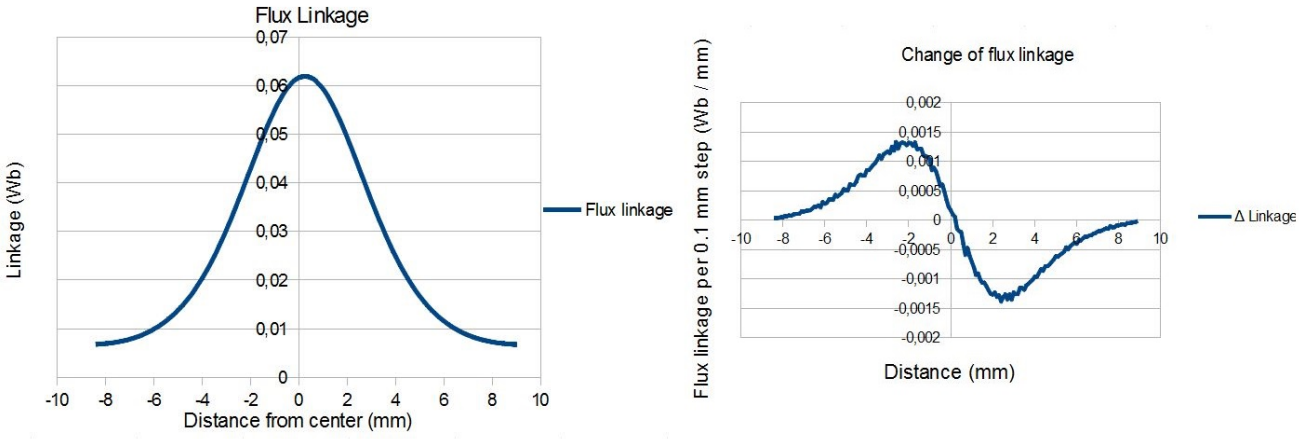

Figure 22: Flux linkage and rate of change in 0.1 mm steps in generator.

diameter nylon tubing with 12 mm inner diameter. A groove was machined on the outer diameter to hold the coiling in place. Inner diameter of the groove was 14 mm and height 3 mm. 0.1 mm diameter wire was used to build the coil. To determine the number of turns in coil, coil resistance was measured to determine the length of wire and number of turn was calculated using known length of loop turn and total length of wire. Coil resistance was 42 ohms as the resistance of wire is approximately 2.2 ohms / meter the total length is approximately 19 meters. As one loop has length of 44 mm, coil had roughly 400 turns.

The prototype was connected on a Brüel Kjær shaker type 4905 and driven using Brüel Kjær power amplifier type 2707. Input signal was generated using NI-USB6218 DAQ and output was measured directly from leads of the generator. Vertical displacement of generator was limited to $7.5mm$. Output signal was a sine wave with amplitude of 5 volts, which was amplified by gain of 8 above frequencies of 30 Hz. At lower frequencies the gain was limited to stay within allowed displacement. Measured graphs are shown in figure 23.

At low frequencies the magnets do not overcome friction and only measurement noise is present in signal. In addition to white noise in measurement there is

3.4 Piezoelectric harvester design

A previous work by

3.5 Hybrid harvester design

3.6 Electronic design

3.6.1 Simulation of circuit

The analog sections of circuit were simulated using LTSpice IV [25]. Microcontroller, radiolink and accelerometer were simulated as resistive load. Battery was modelled as

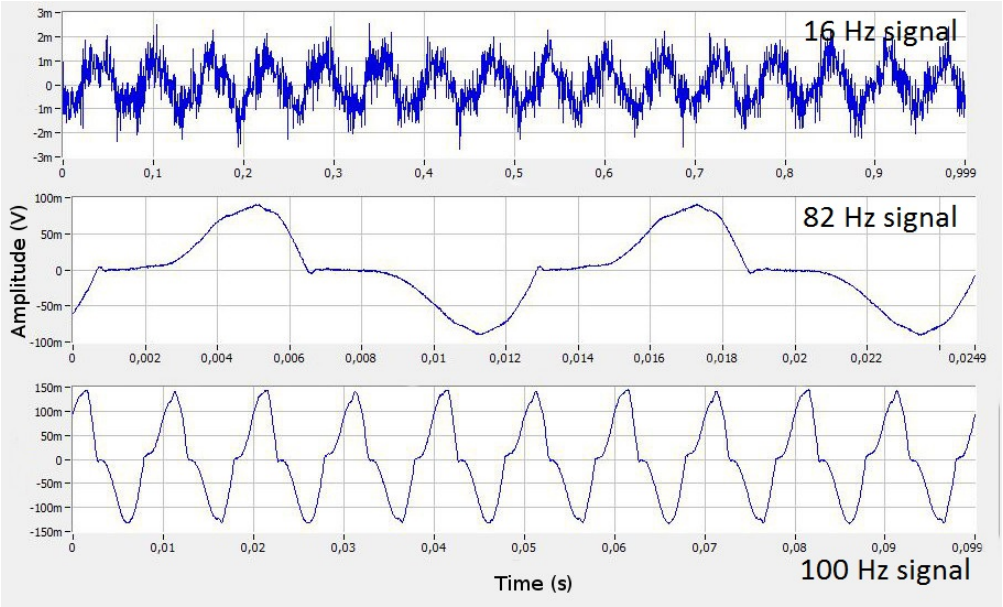

Figure 23: Measured open-loop voltage outputs at various frequencies

a voltage source with high-value capacitor and low-value resistor in series. Piezoelectric harvesting was modelled both as high-voltage source with capacitor in series and current source with capacitor in parallel. Electromagnetic harvesting was modelled as low-impedance low-voltage source.

once lookup-tables can be generated, create maximum power point tracking. LTC3331 presents an interesting opportunity for maximum power point tracking (MPPT). While the impedances of individual components cannot be tuned in real-time, the microcontroller can determine rotation frequency of tyre from accelerometer readings and determine the maximum power point. LTC3331 can adjust the target voltage for energy storage buffer capacitor, which enables MPPT-control of system.

The simulation model is shown in figure 24. Connections were adjusted as needed to generate simulation data for different purposes, such measuring energy efficiency, transient response, MPPT etc.

–simulated efficiency –simulated mppt –figures

3.6.2 Schematic design

The printed circuit board (PCB) schematic is a logical representation of the components and how they connect to each other. The schematic is designed in accordance to datasheets, reference designs and application notes of main circuit components. As the design operates in high-vibration environment with wide temperature variations, special care is used to select components which have well-defined temperature and mechanical characteristics.

As the circuit is a low-power design, careful attention has to be paid to parasitic properties and non-ideal behaviour of components. For example electrolytic capacitor

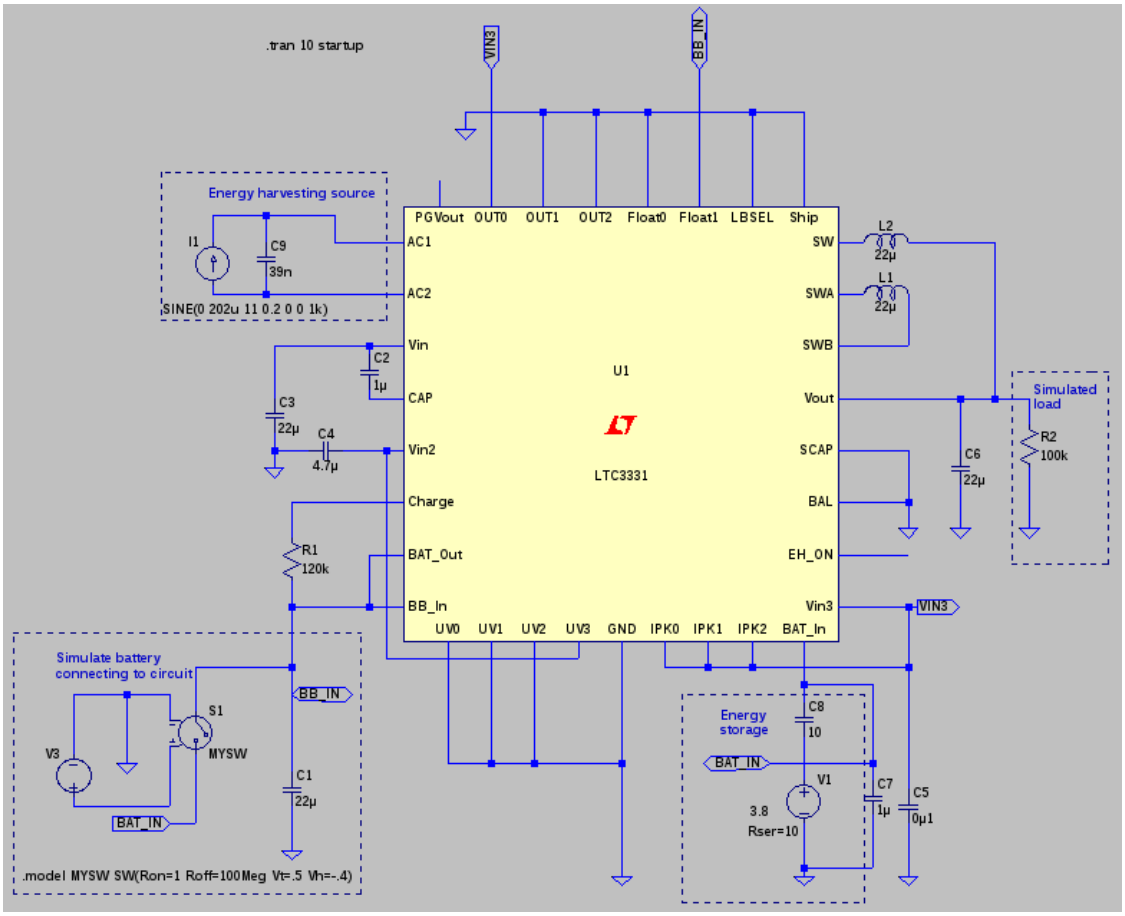

Figure 24: LTSpice [25] simulation of electrical circuit

can have leakage current of several microamperes [9], which is in the same order of magnitude as the targeted sleep current consumption of system. Likewise any signalling current should be kept at minimum.

Another important point of view is the modularity and testability of the circuit. All critical lines have provision for testing and debugging for development and verification of circuit functionality. Figure 25 shows the interconnections in system. The power supply can be cut off to separate sections of circuit for current measurement as needed. This has additional benefit of leaving places for power supply filtering components in case some section of circuit emits electrical noise through power supply lines.

Power supply has some conflicting requirements, as any noise in power degrades radio and measurement performance, but on the other hand the power supply should be efficient switch mode power supply to keep power consumption at minimum. LTC3331 has switch-mode power supplies which can be used to generate supply rails for the rest of circuit, these are used and noise is dealt with by passive filtering. Most of the power supply design 26 is relatively straightforward application of ideas presented in LTC3331 datasheet, but a few special considerations have been given to tailor the power supply for application. Device is configurable by soldering

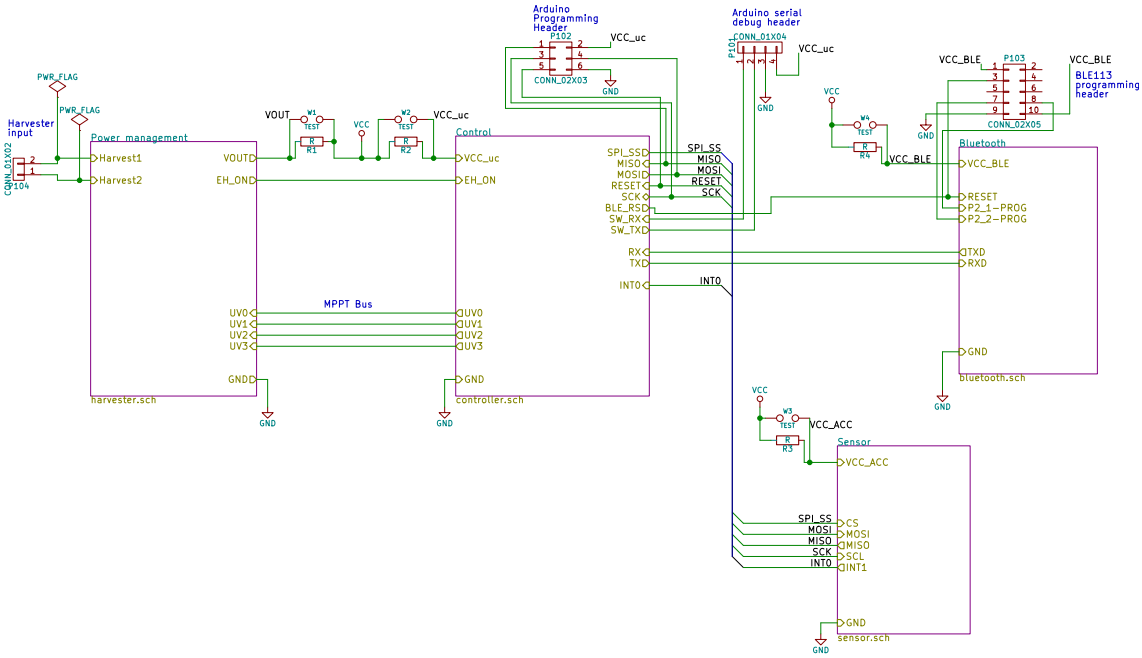

Figure 25: System level design of electronics

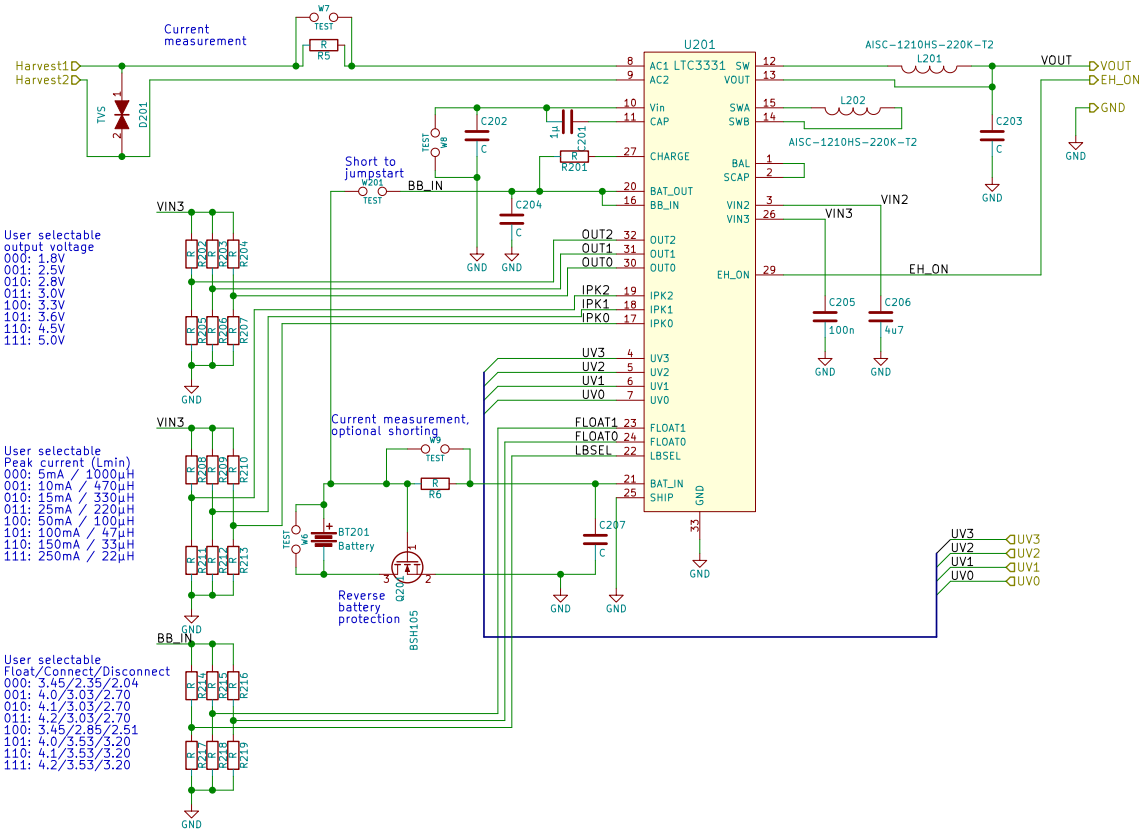

Figure 26: Power supply with harvesting input, battery management and SMPS voltage output.

appropriate resistors, and the energy harvesting MPPT can be controlled by external microcontroller using signals UV[0:3].

Battery configuration allows different chemistries to be tested, as the under- and overvoltage lockout levels are user selectable. If a non-rechargeable battery is desired, battery charging can be disabled by omitting resistor R201.

Central controller is built around ATMEGA328 [4] microcontroller. The controller uses SPI and UART serial communication between sections of the system, and it has parallel connection to LTC3331 to set the energy harvester voltage levels for MPPT. LTC3331 has EH_ON output, which rises to logic high level of approximately 4.8 volts when the circuit is being supplied by harvested energy rahter than by a battery. This voltage level is above the circuit supply voltage, and therefore interfacing it directly to ATMEGA328 would be damaging. Interfacing is done by N-MOSFET BSH105 [36] and internal pullup-resistor on ATMEGA328. When harvested energy is available, pull-up of ATMEGA328 becomes grounded through BSH105. This causes somewhat significant current leakage, in range of tens of microamperes while pull-up is being pulled down. However this leakage is present only while harvested energy is available, so it will not drain the battery of circuit. While harvested energy is not available, the MOSFET is shut off. Special care was taken to select a model of MOSFET with small off leakage to avoid drain while system is being run on battery

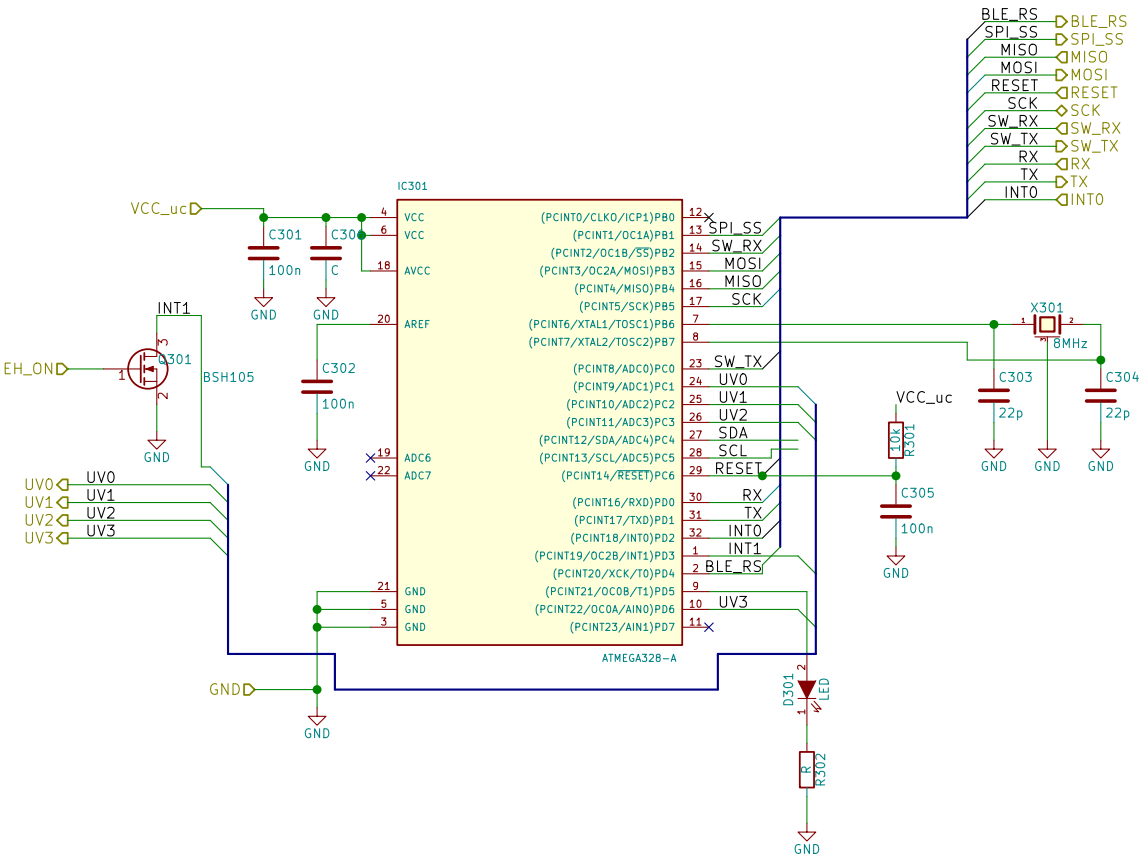

Figure 27: Control circuit with external interrupts from sensor and energy harvesting.

power, BSH105 is specified to have leakage in range of tens of nanoamperes.

Most important power saving is achieved through careful design of software. Sleep power states of ATMEGA328 consume miniscule amount of power when compared to active state, therefore minimizing active time of circuit is a high priority. If the program is not CPU time limited, clock rate can be scaled down to 1 MHz using internal clock divider. Maximum CPU frequency can be incresed by selecting another crystal, but increasing clock frequency will require higher supply voltage which in turn leads to higher overall power consumption in entire system.

Radio link is implemented with BLE113 module. The module could act as stand-alone controller for the system, but radio link has been separated from control logic to allow focused study of different sections of circuit. Schematic 28 is very simple, power supply is decoupled by bypassing capacitors as recommended by datasheet and programming header has been brought out. Communication to microcontroller is handled by universal asynchronous receiver/transmitter (UART) communication using 2.5 V level signaling.

BLE113 can be forced to sleep by external control if needed and it can operate autonomously while main controller is sleeping. Data payload can be up to 20 bytes per packet as specified by BLE protocol cite, maximum data throughput is defined by connection interval. As transmitting data consumes active time and therefore power, data transmissions should be minimized while harvested energy is not available.

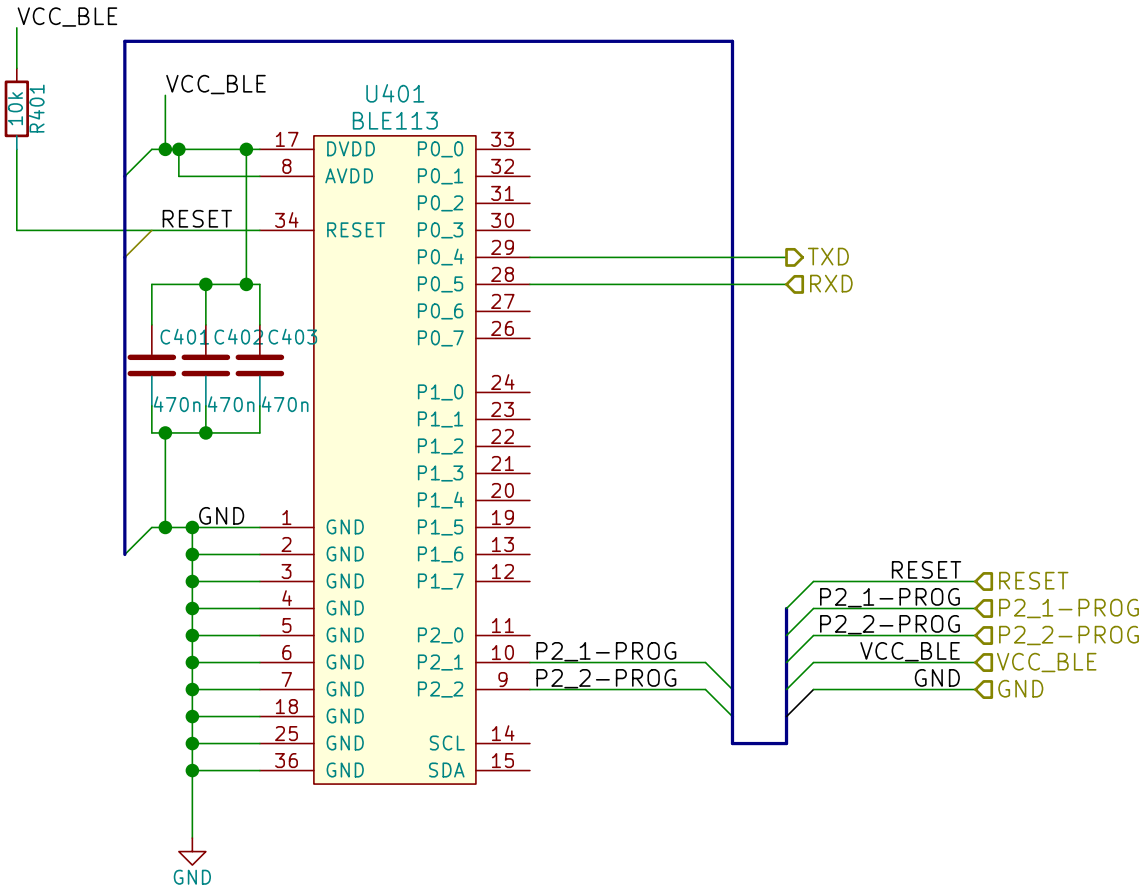

Figure 28: Bluetooth connectivity built with BLE113 module

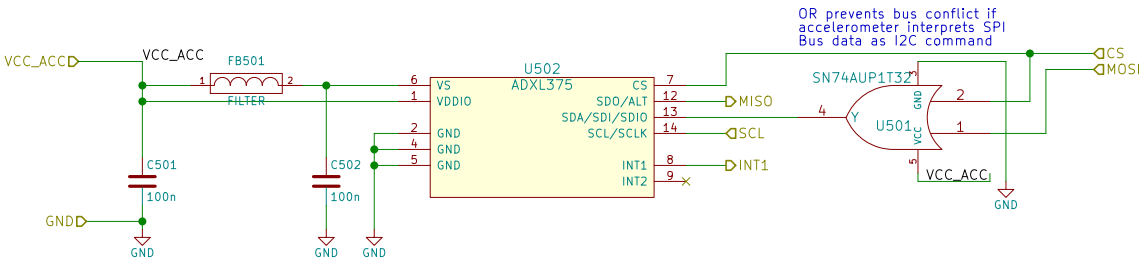

Figure 29: Accelerometer circuit

There is an accelometer ADXL375 onboard the PCB to study applications of tyre sensor system. Schematic of sensor section is shown in figure 29. The power supply section has a separate digital Input/Output (IO) supply voltage which is further filtered for analog sections of board by FB501 and C502. Both supplies are fed by same system level power bus from LTC3331.

ADXL375 is capable of both SPI and I2C communication, SPI communication was selected to facilitate faster communication to minimize time control circuit has to be in awake and to avoid additional power drain through the required pull-up resistors of I2C bus. On the other hand, the circuit has a design feature which requires usage of OR gate to avoid SPI sequence being interpreted as I2C command. The OR was selected to be SN74AUP1T32 [41], which has minimal static power current consumption of 0.1 microamperes.

As the circuit will be subject to extreme accelerations, all the components are surface mounted. This gives maximal solder pad area to height ratios, which helps to maintain the integrity of circuit. Larger components, such as inductors can be additionally glued for increased mechanical reliability.

table to sum expected ON times and power consumption?

3.6.3 Circuit layout

The PCB layout defines the physical placement of the components on the circuit board. Usually circuits are laid out by defining the outline of the board. Then any mechanical constraints, such as mounting holes and connectors are placed. Next step is to place the main ICs. As the main features of circuit are defined, subsections of circuit is planned. Critical and sensitive components such as crystals and antennas are placed as first priority. Then the power supply lines and power supply components are placed, in this case the inductors and capacitors of SMPS are placed as close as possible to relevant pins.

The circuit is laid out on 4-layer PCB, where inner layers are dedicated to ground and power planes. This means that power supply decoupling needs a lot less care than on 2-layer board, generally a via straight from power pin to relevant plane gives low-impedance supply to circuit. Power supply decoupling capacitors are still placed as close as possible to relevant pins and power supplies are fed directly from capacitors when possible to minimize power supply noise leaking into power planes.

Finally the rest of the circuit is laid out. As the currents flowing on board are

relatively small and signal rates are low, routing can be rather carefree on non-critical sections. Final board is shown in figure 30.

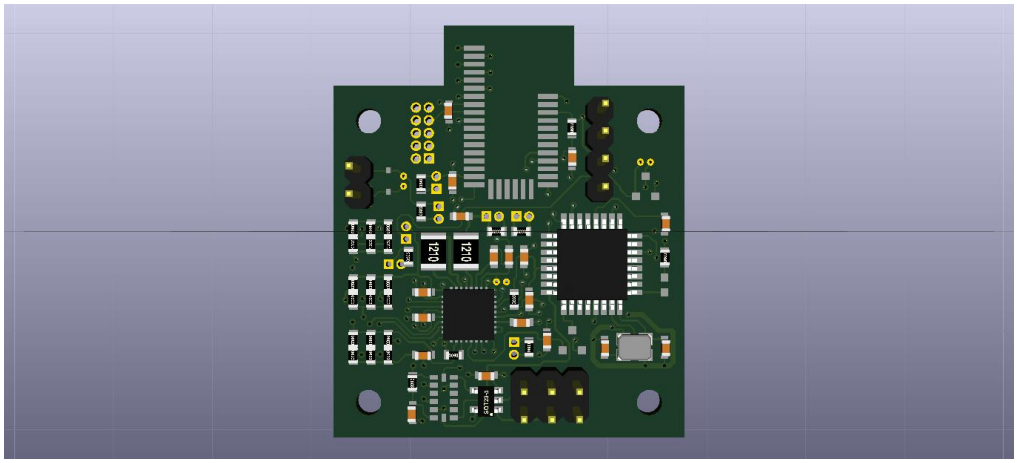

Figure 30: Render of the final PCB

In addition to mechanical and electrical properties, the PCB also acts as heat sink for mid-power components. In this circuit only LTC3331 needs special attention to thermal design, it is cooled by several vias under the pad of circuit into ground plane. As copper is excellent conductor for heat, any thermal output from LTC3331 gets coupled to groundplane where it can spread to a wider area.

3.7 Mechanical design of generator

Material for the shaft has a few requirements. It has to have at least as good temperature characteristics as the magnet being used and it must be hard enough to not deform under impacts. Low friction coefficient is desirable as this leads to smaller losses, and long time durability under wear is of course desired. Being lightweight and easily machinable are also desired characteristics. As the generator is small, volumetric cost of the material is of little concern. For the electro-magnetic generator design material ferromagnetism has to be considered. Table 3 has comparison of different materials considered for the application.

Table 3: Materials for the shaft of generator [37], [14].

Material	**Hardness**	**Friction**	**Durability**	**Temperature**
PTFE(Teflon)	Very low	Lowest	Lowest	-190... + 250 °C
Polycarbonate	Very high	High [18]	-	-60... + 125 °C
PA 6 (Nylon)	Low	Medium	High	-40... + 80 °C
Oil-infused Nylon	Low	Very low	Very high	-20... + 105 °C
Acryllic	High	-	-	-40... + 70 °C
Polyacetal (POM C)	Medium	Low	Low	-50... + 105 °C

4 Results

4.1 Validation of harvester electrical model

A Simulink model was built to verify feasibility of the linear generator. The simulation included real acceleration data from previous studies made by cite and a model of generator as well as a simplified capacitive-resistive load. There is an abundance of previous work done on simulating linear generators cite, however a simplified model was used at this stage to get a proof-of-concept level generator. Further work remains in optimizing the design in terms of size, mass, power output, usable speed range, cost and long-term reliability.

4.2 Validation of harvester mechanical model

Text on estimating and measuring mechanical friction and strength of device.

4.3 Electrical performance of circuit

Text on measured electrical parameters, current and power consumption, timings, power supply efficiency etc.

4.4 System-level performance

Text on integration, testing inside tyre and test drive on real road.

5 Conclusions

In this paper the operation environment of tyre has been presented, and reasonable choices for energy harvesting technology have been identified. Both Piezoelectric and electromagnetic methods have been researched. While both methods can produce similar AC-power levels to resistive load, electromagnetic harvesting was found to produce too low voltage for rectification and operation of microcontroller.

Various voltage doubling and active rectification schemes do exist, as well as boost converters and charge pumps which could be used to bring voltage from electromagnetic harvesting to usable levels. However, piezoelectric harvester does not require such extra complexity.

Future work is needed on determining which factors limit the voltage output of electromagnetic harvester below the simulated results as well as to create maximum power point tracking for both methods. In addition, identical test setups will be created to compare the power output of final electromagnetic and piezoelectric generator power levels.

References

[1] R. Amatya and R. J. Ram. Solar thermoelectric generator for micropower applications. *Journal of Electronic Materials*, 39(9):1735–1740, 2010.

[2] Djilali Amrani. Determination of Magnetic Dipole Moment of Permanent Disc Magnet with Two Different Methods. 2015.

[3] E. Arroyo, a. Badel, F. Formosa, Y. Wu, and J. Qiu. Comparison of electromagnetic and piezoelectric vibration energy harvesters: Model and experiments. *Sensors and Actuators, A: Physical*, 183(June):148–156, 2012.

[4] Atmel. ATMEL 8-BIT MICROCONTROLLE R WITH 4/8/16/32KBYTES IN-SYSTEM PROGRAMMABLE FLASH. 2014.

[5] Bluegiga. BLE113 data sheet (v1.2). (November), 2013.

[6] S Boisseau, G Despesse, and B Ahmed Seddik. Electrostatic Conversion for Vibration Energy Harvesting. *Small-Scale Energy Harvesting*, pages 1–39, 2012.

[7] I. Boldea and S. a. Nasar. Linear electric actuators and generators. *IEEE Transactions on Energy Conversion*, 14(3):712–717, 1999.

[8] I. Boldea and S. a. Nasar. *Linear electric actuators and generators*, volume 14. 1999.

[9] Jens Both. Leakage current properties of modern electrolytic capacitors.pdf. Technical report, 2001.

[10] C. R. Bowen and M. H. Arafa. Energy Harvesting Technologies for Tire Pressure Monitoring Systems. *Advanced Energy Materials*, pages n/a–n/a, 2014.

[11] Shuo Cheng and David P Arnold. A multi-pole magnetic generator with enhanced voltage output for low-frequency vibrational energy harvesting. *PowerMEMS 2008+ microEMS 2008*, pages 125–128, 2008.

[12] John C Elmes. Maximum Energy Harvesting Control for Oscillating Energy Harvesting Systems. page 84, 2005.

[13] Alper Erturk, Daniel J Inman, Scott L Hendricks, Michael W Hyer, and Ishwar K Puri. Electromechanical Modeling of Piezoelectric Energy Harvesters. *Health San Francisco*, 2009.

[14] ETRA. TEKNISET MUOVIT, 2015.

[15] Feng Ru Fan, Zhong Qun Tian, and Zhong Lin Wang. Flexible triboelectric generator. *Nano Energy*, 1(2):328–334, 2012.

[16] R W Fox, A T McDonald, and P J Pritchard. *Introduction to Fluid Mechanics*. 2008.

[17] a N Gent and J D Walter. The Pneumatic Tire. *Rubber World*, (February):707, 2005.

[18] Goodfellow. Polycarbonate (PC).

[19] S Jacob, V Ramanarayanan, R Karunanithi, C Damu, and G Jagadish. Development of a Moving Magnet Linear Motor Pressure Wave Generator for a Pulse Tube Refrigerator. m:361–370, 2011.

[20] Panida Jirutitijaroen. EE2022 Electrical Energy Systems Lecture 10 : Electric Power Generation – an Equivalent Circuit of a Generator. 2012.

[21] Kensuke Kanda, Takashi Saito, Yuki Iga, Kohei Higuchi, and Kazusuke Maenaka. Influence of parasitic capacitance on output voltage for series-connected thin-film piezoelectric devices. *Sensors (Switzerland)*, 12(12):16673–16684, 2012.

[22] S H Kim, S Ju, C H Ji, and S J Lee. Equivalent circuit model of an impact-based piezoelectric energy harvester. *Journal of Physics: Conference Series*, 557:012094, 2014.

[23] Ali E. Kubba and Kyle Jiang. A comprehensive study on technologies of tyre monitoring systems and possible energy solutions. *Sensors (Switzerland)*, 14(6):10306–10345, 2014.

[24] B Y Amit Lal and James Blanchard. The daintiest of dynamos. *IEEE Spectrum*, (September):36–41, 2004.

[25] Linear Technology. LTSpice IV.

[26] M Löhndorf, T Kvisterø y, E. Westby, and E Halvorsen. Evaluation of Energy Harvesting Concepts for Tire Pressure Monitoring Systems. *International Workshops on Micro and Nanotechnology for Power Generation and Energy Conversion Applications*, pages 331–334, 2007.

[27] G Manla, N.M White, and J Tudor. Harvesting energy from vehicle wheels. *Solid-State Sensors, Actuators and Microsystems Conference, 2009.*, 2009.

[28] Mika J Matilainen and Ari Juhani Tuononen. Intelligent Tire to Measure Contact Length in Dry Asphalt and Wet Concrete Conditions. *Avec 12*, pages 1–6, 2012.

[29] Medhat K Bahr Khalil. Estimated versus Calculated Viscous Friction Coefficient in Spool Valve Modeling. pages 1–9, 2008.

[30] David Meeker. Finite Element Method Magnetics, Version 4.2, 2013.

[31] K M Mossi, R P Bishop, R C Smith, and H T Banks. Evaluation Criteria for THUNDER Actuators 2 . Typical THUNDER Configurations. pages 1–6.

[32] Arto J. Niskanen and Ari J. Tuononen. Three 3-axis accelerometers fixed inside the tyre for studying contact patch deformations in wet conditions. *Vehicle System Dynamics*, 52(sup1):287–298, 2014.

[33] T O'Donnell, Chitta Saha, Steve Beeby, and John Tudor. Scaling effects for electromagnetic vibrational power generators. *Microsystem Technologies*, (April):26–28, 2007.

[34] Joseph a. Paradiso and Thad Starner. Energy scavenging for mobile and wireless electronics. *IEEE Pervasive Computing*, 4(1):18–27, 2005.

[35] Deep Patel, Rohan Mehta, Rhythm Patwa, Sahil Thapar, and Shivani Chopra. RF Energy Harvesting. *International Journal of Engineering Trends and Technology (IJETT)*, 16(8):382–385, 2014.

[36] Philips Semiconductors. BSH105 N-channel enhancement mode MOS transistor. Technical report, 1998.

[37] Plastics International. Hardness Scale - Durometer Comparisons of Materials, 2015.

[38] Data Sheet. Power Digital MEMS Accelerometer. pages 1–32, 2012.

[39] Kanwar Bharat Singh, Vishwas Bedekar, Saied Taheri, and Shashank Priya. Piezoelectric vibration energy harvesting system with an adaptive frequency tuning mechanism for intelligent tires. *Mechatronics*, 22(7):970–988, 2012.

[40] Linear Technology. LTC3331 - Nanopower Buck-Boost DC/DC with Energy Harvesting Battery Life Extender. pages 1–32.

[41] Texas Instruments. SN74AUP1T32. 2010.

[42] S. Tornincasa, M. Repetto, E. Bonisoli, and F. Di Monaco. Energy harvester for vehicle tires: Nonlinear dynamics and experimental outcomes. *Journal of Intelligent Material Systems and Structures*, 23(1):3–13, 2012.

[43] L Wang and F-G Yuan. Structural Vibration Energy Harvesting by Magnetostrictive Materials (MsM). *4th China-Japan-US Symposium on Structural Control and Monitoring*, pages 1–8, 2006.

[44] Hugh D. Young and Roger A. Freedman. *University Physics*. Pearson, 12th edition, 2008.

[45] Qi Zhang, Amen Agbossou, Zhihua Feng, and Mathieu Cosnier. Solar micro-energy harvesting with pyroelectric effect and wind flow. *Sensors and Actuators, A: Physical*, 168(2):335–342, 2011.